

Dynamical freeze-out criterion in hydrodynamical description of $Au + Au$ collisions at $\sqrt{s_{AA}} = 200$ GeV and $Pb + Pb$ collisions at $\sqrt{s_{AA}} = 2760$ GeV.

Saeed Ahmad^a, Hannu Holopainen^b and Pasi Huovinen^{b,c}

^a*STEM Division, Eastfield College, 3737 Motley Drive, Mesquite, TX 75150, USA*

^b*Frankfurt Institute for Advanced Studies, Ruth-Moufang-Str. 1, D-60438 Frankfurt am Main, Germany and*

^c*Institute of Theoretical Physics, University of Wrocław, pl. M. Borna 9, PL-50204 Wrocław, Poland*

(Dated: November 6, 2018)

In hydrodynamical modeling of ultrarelativistic heavy-ion collisions, the freeze-out is typically assumed to take place at a surface of constant temperature or energy density. A more physical approach is to assume that freeze-out takes place at a surface of constant Knudsen number. We evaluate the Knudsen number as a ratio of the expansion rate of the system to the pion scattering rate, and apply the constant Knudsen number freeze-out criterion to ideal hydrodynamical description of heavy-ion collisions at RHIC ($\sqrt{s_{AA}} = 200$ GeV) and the LHC ($\sqrt{s_{AA}} = 2760$ GeV) energies. We see that once the numerical values of freeze-out temperature and freeze-out Knudsen number are chosen to produce similar p_T distributions, the elliptic and triangular anisotropies are similar too, in both event-by-event and averaged initial state calculations.

PACS numbers:

I. INTRODUCTION

The fluid-dynamical description of heavy-ion collisions at BNL Relativistic Heavy Ion Collider (RHIC) and CERN Large Hadron Collider (LHC) has been very successful in reproducing the observed particle distributions and their anisotropies at low values of transverse momentum [1–3]. However, since what is experimentally observed is not a particle fluid, but individual particles, the fluid dynamical description must break down at some point during the evolution, the interactions must cease, and the particles must start behaving like free-streaming particles instead. The particles decouple from the fluid, and their momentum distributions freeze-out—a process appropriately known as decoupling or freeze-out.

When the freeze-out happens is not described by fluid dynamics but has to be decided using some other model or theory. Fluid dynamics is considered to be valid when the ratio of the microscopic to macroscopic scales of the system—its Knudsen number—is much smaller than one. In the context of heavy-ion collisions, fluid dynamics has traditionally been considered to be valid until either the mean free path of particles exceeds the size of the system, or the expansion rate exceeds the collision rate of the particles [4, 5]. The Knudsen number can be defined in several ways [6], and thus both of these dynamical criteria are equivalent to the requirement that the Knudsen number is less than one. The idea of using the scattering and expansion rates as the limit for the validity of fluid dynamics, and thus as a decoupling criterion, is an old one [7], but it has been used in fluid-dynamical calculations only a couple of times [8–12]. Instead, the freeze-out is assumed to take place on a surface of constant temperature (or density). It has been argued that since the scattering rate depends strongly on temperature ($\propto T^3$ for a constant cross section), the freeze-out is a very fast process, and thus a constant temperature surface is a good approximation to the constant Knudsen

number surface [4, 13, 14].

It was seen in earlier studies with optical Glauber initial profiles that, while the constant Knudsen number surface differs significantly from the constant temperature surface, the effect on observable particle p_T distributions is small [11] and that elliptic flow of charged hadrons shows sensitivity to the freeze-out criterion only at large values of transverse momentum or rapidity, or in peripheral collisions [12]. However, in contemporary event-by-event hydrodynamical calculations, the flow develops more violently and more unevenly than when an averaged initial state is used [15]. Thus it is not obvious whether the two freeze-out conditions lead to similar particle distributions when the initial density fluctuates event-by-event. Furthermore, the evaluation of the Knudsen number in Refs. [11, 12] was based either on pion-pion scattering ignoring all other scattering processes and the chemical non-equilibrium during the hadronic stage [11], or on assumed temperature dependence of the shear viscosity coefficient [12]. Thus it is unknown how more sophisticated calculations of the microscopic scale would affect the results.

In this work we further study whether the freeze-out criterion has any observable effects. We evaluate the p_T differential elliptic flow $v_2(p_T)$ of identified particles (pions and protons) in $\sqrt{s} = 200$ GeV $Au + Au$ (RHIC) and $\sqrt{s} = 2760$ GeV $Pb + Pb$ collisions (LHC) using both constant temperature and constant Knudsen number freeze-out criteria. To test our assumption that the large gradients in event-by-event calculations would make the system more sensitive to the freeze-out criterion, we model the collisions at RHIC both event-by-event and using the averaged initial state. We use the pion scattering rate as the microscopic scale, and calculate the rate in a chemically frozen hadron gas from scattering cross sections, including scatterings with all hadron species. Since our aim is not a faithful reproduction of the data, we simplify the description by using a simple boost-invariant

ideal fluid model.

Note that in this work we use the conventional Cooper-Frye description (see Sect. III B) to evaluate the particle distributions at freeze-out. We do not address the negative contributions¹, but our approach differs from the conventional freeze-out procedure only by the choice of the decoupling surface.

To some extent the freeze-out problem has been solved in so-called hybrid models, where the late stage of the evolution is described using a Boltzmann transport model [18, 19]. Nevertheless, the results in these models depend on when the switch from fluid to cascade is made [18, 20], and therefore it is interesting to study how different criteria for particlization surface affect the particle distributions even in the context of hybrid models.

II. DYNAMICAL FREEZE-OUT CRITERION AND SCATTERING RATE

To maintain kinetic equilibrium in an expanding system the scattering rate must be much larger than the expansion rate. We express this condition as

$$\text{Kn} = \frac{\theta}{\Gamma} \ll 1, \quad (1)$$

where Γ is the scattering rate and θ is the hydrodynamical expansion rate. When Kn approaches one, there are not enough collisions to maintain the kinetic equilibrium, and the system freezes-out. Since Kn is a ratio between (an inverse of) a macroscopic length scale and (an inverse of) a microscopic length, it can be identified as a Knudsen number, which should be much smaller than one for fluid dynamics to be valid. Based on these considerations we define a dynamical freeze-out criterion as a surface of constant Knudsen number $\text{Kn} = \text{Kn}_f$, where $\text{Kn}_f \sim 1$.

Before one can apply this criterion, the scattering rate must be known. We evaluate the pion scattering rate

¹ For a recent discussion see Refs. [16, 17].

² See the discussion about “pion wind” in Ref. [9].

in hadron resonance gas and use it in our freeze-out criterion for all particles. One could argue that we should calculate the scattering rate individually for each particle species and decouple them separately at the corresponding Knudsen number. However, in order to be consistent, one should also remove the decoupled particles from the fluid and model the interaction between the fluid and the removed particles², which are not in equilibrium anymore. This cannot be consistently implemented (at least not easily) in the hydrodynamical framework and thus we make the simplifying assumption that the whole system decouples when the most abundant particles, *i.e.* pions, do.

A. Scattering rate of pions

Here we calculate the average scattering rate of pions in hadron resonance gas in kinetic equilibrium. The rate is obtained from [21–24]

$$\Gamma = \frac{1}{n_\pi(T, \mu_\pi)} \sum_i \int d^3 p_\pi d^3 p_i f_\pi(T, \mu_\pi) f_i(T, \mu_i) \times \frac{\sqrt{(s-s_a)(s-s_b)}}{2E_\pi E_i} \sigma_{\pi i}(s), \quad (2)$$

where n_π is the density of pions, $f_{\pi/i}(T, \mu_{\pi/i})$ is the thermal distribution function of pions/particle i , T being temperature and $\mu_{\pi/i}$ the chemical potential of pion/particle i . $\sqrt{(s-s_a)(s-s_b)}/(2E_\pi E_i)$ is the relative velocity when s is the square of the center-of-mass energy, $s_a = (m_\pi + m_i)^2$, $s_b = (m_\pi - m_i)^2$, and $E_{\pi/i}$ and $m_{\pi/i}$ are the energy and mass of pion/particle i , respectively. The pion-particle i scattering cross section is labeled $\sigma_{\pi i}$ and the sum runs over all particle species included in the equation of state (EoS) [25].

One can perform most of the integrals analytically and, after some algebra (See Appendix A), one arrives at:

$$\Gamma = \frac{T}{n_\pi(T, \mu_\pi)} \sum_i \frac{g_i}{32\pi^4} \sum_{k=1}^{\infty} e^{k\mu_\pi/T} \sum_{n=1}^{\infty} \frac{(\mp 1)^{n+1}}{n} e^{n\mu_i/T} \times \int_{s_a}^{\infty} ds \frac{\sigma_{\pi i}(s)(s-s_a)(s-s_b)}{\sqrt{rs - (r-1)(m_i^2 - rm_\pi^2)}} K_1\left(\frac{n}{T} \sqrt{rs - (r-1)(m_i^2 - rm_\pi^2)}\right), \quad (3)$$

where g_i is the degeneracy of particle i , and $r = k/n$.

Cross sections are evaluated as in the UrQMD model [26, 27]. Thus the largest contribution comes from resonance formation, which is evaluated using the Breit-

Wigner formula:

$$\sigma_{\pi i \rightarrow R}(s) = \frac{2g_R + 1}{(2g_\pi + 1)(2g_i + 1)} \frac{\pi}{(p_{\text{cms}}(\sqrt{s}))^2} \times \frac{\Gamma_{R \rightarrow \pi i}(\sqrt{s}) \Gamma_{\text{tot}}(\sqrt{s})}{(m_R - \sqrt{s})^2 + \Gamma_{\text{tot}}^2(\sqrt{s})/4}, \quad (4)$$

where $g_{R/\pi/i}$ are the degeneracies of the resonance/pion/particle i , and p_{cms} is the center of mass momentum of the scattering partners (See Appendix B). $\Gamma_{\text{tot}}(M)$ is the full decay width obtained as a sum of all mass dependent partial decay widths $\Gamma_{i,j}(M)$ (See Appendix C) given by

$$\Gamma_{R \rightarrow \pi i}(M) = \Gamma_R^{\pi i} \frac{m_R}{M} \left(\frac{p_{\text{cms}}(M)}{p_{\text{cms}}(m_R)} \right)^{2l+1} \times \frac{1.2}{1 + 0.2 \left(\frac{p_{\text{cms}}(M)}{p_{\text{cms}}(m_R)} \right)^{2l}}, \quad (5)$$

where $\Gamma_R^{\pi i}$ is the partial decay width of the resonance into the πi channel at the pole, l the decay angular momentum of the exit channel, and m_R the pole mass of the resonance. The pole masses and the decay widths are taken from the Particle Data Book [28] as implemented in the calculation of the EoS [25].

In addition we assume elastic meson-meson scatterings with cross section $\sigma_{mm} = 5$ mb and elastic $\pi\pi$ scatterings with $\sigma_{\pi\pi} = \sigma_0 \exp(-(\sqrt{s} - m_0)^2/w)$ where $\sigma_0 = 15$ mb, $m_0 = 0.65$ GeV, and $w = 0.1$ GeV. With these choices we are able to reproduce the measured pion-pion, pion-kaon, and pion-nucleon scattering cross sections reasonably well.

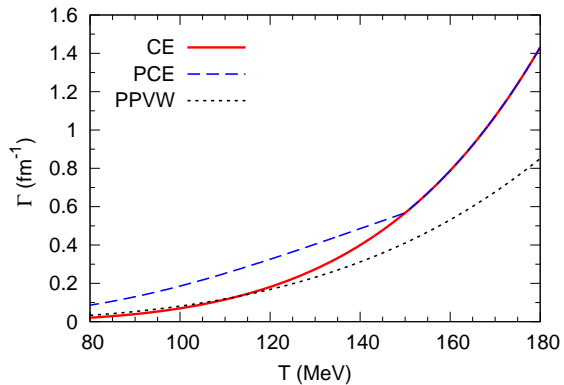


FIG. 1: The scattering rate of pions in both chemically equilibrated (CE, red solid line) and chemically frozen (PCE, blue dashed line) hadron resonance gas compared to the parametrization [29] of the rate evaluated in Ref. [23] (PPVW, black dotted line).

In Fig. 1 we compare the evaluated scattering rates to the rates calculated in Ref. [23]. At low temperatures our simple approach agrees with the more sophisticated calculation of Ref. [23], but above $T \approx 120$ MeV temperature our rate is larger simply because we include more states in the calculation, and thus the density of scattering partners is larger at large temperatures. Moreover, the scattering rate in a chemically frozen hadron gas is larger than that in a chemically equilibrated hadron gas due to larger particle densities.

III. HYDRODYNAMICAL FRAMEWORK

We use an updated version of the event-by-event ideal hydrodynamical framework developed in Ref. [15].

A. Ideal hydrodynamics

We solve the ideal hydrodynamical equations

$$\begin{aligned} \partial_\mu T^{\mu\nu} &= 0, \\ \partial_\mu j^\mu &= 0, \end{aligned} \quad (6)$$

where $T^{\mu\nu} = (\epsilon + P)u^\mu u^\nu - Pg^{\mu\nu}$ is the ideal energy-momentum tensor, $j^\mu = n_B u^\mu$ the net-baryon current, ϵ is the energy density, P is the pressure, u^μ is the fluid four-velocity and n_B the net-baryon density. We use two different equations of state (EoS): (i) *s95p-v1*, which is always in chemical equilibrium, and (ii) *s95p-PCE-v1*, which has a chemical freeze-out at temperature $T_{\text{chem}} = 150$ MeV [25]. Both of these EoSs assume zero net-baryon density.

We concentrate on the mid-rapidity region, where boost-invariance is a reasonable assumption at the LHC and full RHIC energies. This assumption reduces the number of dimensions in evolution equations to 2+1. We use the sharp and smooth transport algorithm (SHASTA) [30] to solve the equations in hyperbolic coordinates, where one uses $\tau = \sqrt{t^2 - z^2}$ and $\eta_s = \frac{1}{2} \log \frac{t+z}{t-z}$ instead of time t and longitudinal coordinate z . At the antidiffusion stage of SHASTA we use DeVore limiter [31], which is a modified version of the Zalesak multidimensional limiter [32].

B. Freeze-out

We employ two different freeze-out criteria. One is the conventional constant temperature criterion, and the other the dynamical criterion, where we assume freeze-out at constant Knudsen number Kn . The hydrodynamical expansion rate is needed to obtain the Knudsen number, and in the boost invariant case it is calculated as [33]

$$\theta = \partial_\mu u^\mu = \partial_\tau u^\tau + \partial_x u^x + \partial_y u^y + u^\tau / \tau. \quad (7)$$

In both cases the freeze-out surface elements $d\Sigma_\mu$ are obtained using CORNELIUS++ subroutine [20]. After the surface elements are found, we calculate the thermal spectrum of hadron species i using Cooper-Frye prescription:

$$\frac{d^3 N_i}{d^3 p} = \int_\Sigma d\Sigma_\mu p^\mu f_i(x, p), \quad (8)$$

where $f_i(x, p)$ is the thermal distribution function of hadron i and p^μ is the four-momentum of the hadron. At this stage we use hadron gas EoS at non-zero net-baryon densities to convert the energy and net-baryon density to temperature and chemical potentials. Since the EoS

during the fluid-dynamical evolution does not allow finite net-baryon density, this procedure is not fully consistent, but the violation of conservation laws is very small at RHIC and even smaller at the LHC.

After the thermal distributions of all hadron species have been evaluated, we sample individual hadrons as described in Ref. [15]. All strong and electromagnetic two- and three-particle decays are then calculated, and the daughter particles added to the respective thermal ensembles. Note that unlike in Ref. [15], we no longer use PYTHIA to handle the decays, but evaluate the decays of all the resonances included in the EoS. When evaluating the charged particle multiplicities we sample hadrons within an interval $|y| < 3$ to make sure that at mid-rapidity the system looks boost invariant after the decays as well. However, when we consider the identified particle p_T -spectra and flow coefficients, we take all particles into account regardless of their rapidity to achieve better statistics.

C. Initial state and centrality class definitions

Initial state and centrality classes are defined using a Monte Carlo (MC) Glauber model described in Ref. [15]. Nucleons are randomly distributed to nucleus using a standard two parameter Woods-Saxon potential. Two nucleons from different nuclei do collide if their transverse distance $r_d < \sqrt{\sigma_{NN}}/\pi$, where σ_{NN} is the inelastic nucleon-nucleon cross section. We take $\sigma_{NN} = 42$ mb at $\sqrt{s_{NN}} = 200$ GeV and $\sigma_{NN} = 64$ mb at $\sqrt{s_{NN}} = 2760$ GeV. Here we neglect nucleon-nucleon correlations and finite size effects since their effects on anisotropies at mid-central collisions were found to be very small [34, 35].

Multiplicity is taken to be proportional to the number of ancestors N_{anc} , which is a weighted sum of the number of participants, N_{part} , and the number of binary collisions, N_{bin} , defined as:

$$N_{\text{anc}} = (1 - f)N_{\text{part}} + fN_{\text{bin}}, \quad (9)$$

where f is the fraction of binary collision contribution. This fraction f is chosen to reproduce the centrality dependence of multiplicity.

In principle, when a fit to the multiplicity data is made, one should first generate events with certain f , sort the events according to their centrality, and then calculate the average number of ancestors in each centrality bin. Unfortunately this is a very time consuming procedure because a large number of events must be made for the centrality class definitions. Thus our approach here is to fix the centrality classes using fixed impact parameter intervals. Because average number of participants and binary collisions is now known at each centrality bin, a χ -squared fit can be easily made to fit the ratio f . This approximation is well justified, because average N_{part} and N_{bin} values are not sensitive to the centrality class definition.

After the fraction of binary collisions, f , is determined, we convert the centrality classes to number of ancestors intervals. To fix f , we used the STAR Collaboration data [36] at RHIC, and the ALICE Collaboration data [37] at the LHC. We neglected the most peripheral centrality classes starting from 60% centrality, since we do not expect hydrodynamics to be applicable for peripheral collisions. Our result for RHIC is $f = 0.088$ and at the LHC we obtain $f = 0.17$.

The initial entropy density distribution $s(x, y)$ for a single event is taken to be

$$s(x, y) = \frac{K_{\text{sd}}}{\sqrt{2\pi\sigma^2}} \sum w_i \exp\left(-\frac{(x-x_i)^2 + (y-y_i)^2}{2\sigma^2}\right), \quad (10)$$

where the sum runs over all participants and binary collisions, w_i is the weight ($(1-f)$ for participant and f for binary collision), x_i and y_i are the transverse coordinates of a participant or a binary collision, and σ is a Gaussian smearing parameter controlling the shape of the distribution. The overall normalization constant K_{sd} is fixed to reproduce the observed multiplicity in the 0-5% most central collisions. In this work we use $\sigma = 0.8$ fm. We do not study the dependence of the results on σ because smaller width of the Gaussians leads to a formation of very small scale structures on the constant Knudsen number surface, see Ref. [38]. The scale of these structures is smaller than the mean free path of pions, and thus we do not consider them physical. At this stage we do not consider it worth the effort to improve the freeze-out criterion to remove these structures since further studies should be carried out using viscous hydrodynamics, and dissipation is known to smear small scale structures anyway.

To calculate the average initial state, we average 1000 MC Glauber initial states. In this procedure impact parameters in each event are aligned. We first obtain an averaged entropy density profile and then use the EoS to convert it to energy density profile, which is the actual initial condition for hydrodynamics.

IV. RESULTS

We concentrate on the effects of the freeze-out criterion on particle distributions and their anisotropies and do not aim to faithfully reproduce the data. We compare the calculated p_T distributions to the data to show that our parameter choices are reasonable, but do not compare elliptic flow nor triangular flow with the data to avoid the need to evaluate the anisotropy the same way the particular data set was analyzed.

A. Averaged initial state in $\sqrt{s_{NN}} = 200$ GeV Au+Au collisions at RHIC

To visualize how the freeze-out surface depends on the freeze-out criterion, we show the constant temper-

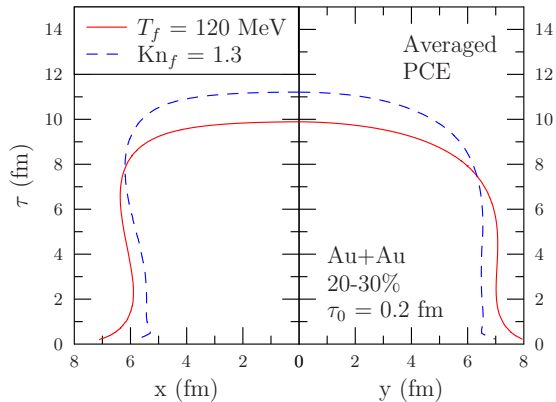


FIG. 2: Constant temperature (solid red curve) and constant Knudsen number (dashed blue curve) freeze-out surfaces in $\sqrt{s_{NN}} = 200$ GeV 20-30% central Au+Au collisions. Surfaces are shown along x - and y -axis.

ature and constant Knudsen number freeze-out surfaces in Fig. 2. The surfaces are calculated using an average initial state for a $\sqrt{s_{NN}} = 200$ GeV 20-30% central Au+Au collision and chemically frozen *s95p*-PCE-v1 EoS. The constant Knudsen number surface is closer to the center of the system, and thus the edges of the system are hotter and the maximum flow velocity is lower than on the constant temperature surface. On the other hand, the system lives longer, and the center decouples at lower temperature. Similar behavior can be seen at the LHC energy as well, and when chemical equilibrium is assumed.

In Fig. 3 we show the transverse momentum spectra of positive pions and protons in 20-30% centrality class. The calculations were performed either using the EoS *s95p*-v1, which assumes chemical equilibrium (Fig. 3 top panel), or the *s95p*-PCE-v1 EoS (Fig 3 bottom panel), which assumes chemical freeze-out at $T_{chem} = 150$ MeV. With *s95p*-v1 EoS the initial time is the conventional $\tau_0 = 0.6$ fm, and the freeze-out temperature $T_f = 140$ MeV and Knudsen number $Kn_f = 1$ lead to almost identical pion and proton distributions which reproduce the data reasonably well.

The assumption of separate chemical freeze-out (Fig. 3 bottom) necessitates the use of an earlier initial time $\tau_0 = 0.2$ fm to make the proton spectrum hard enough³. When chemical equilibrium has been lost, the temperature decreases faster with decreasing energy density than in chemical equilibrium. This necessitates the use of lower freeze-out temperature $T_f = 120$ MeV, and larger freeze-out Knudsen number $Kn_f = 1.3$ to get sufficient

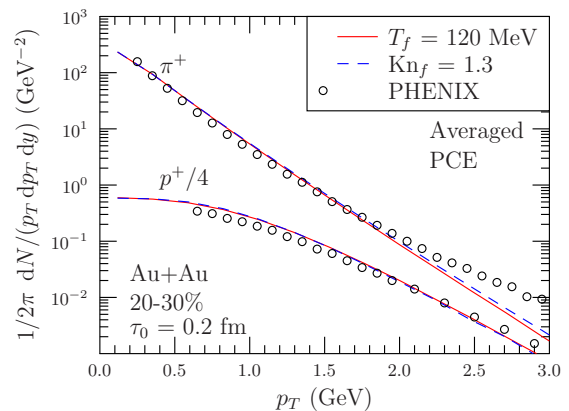
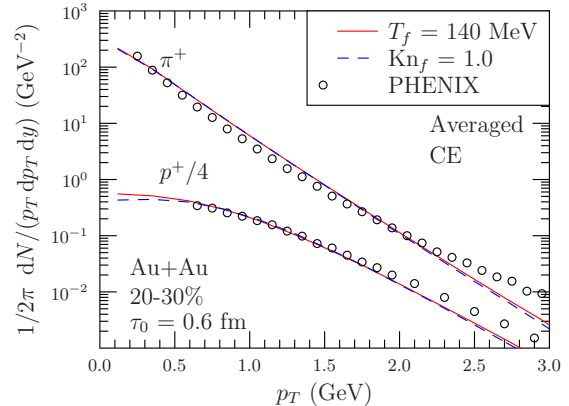


FIG. 3: Transverse momentum spectra of positive pions and protons in $\sqrt{s_{NN}} = 200$ GeV 20-30% central Au+Au collisions assuming chemically equilibrated (top) or chemically frozen (bottom) EoS. The solid red line corresponds to the results obtained using freeze-out at constant temperature and the dashed blue line using freeze-out at constant Knudsen number. The data are from the PHENIX Collaboration [39].

transverse flow to reproduce the data. Since Kn_f is a free parameter of the order of one, and the assumption of chemical equilibrium until the end of the evolution somewhat unphysical, it is acceptable that Kn_f is different for CE and PCE EoSs.

As shown it is possible to find constant temperature and constant Knudsen number values for freeze-out, which give similar pion and proton spectra. This is a non-trivial result, since the corresponding freeze-out surfaces are different. On a constant Knudsen number surface the average flow velocity is lower, and the center decouples at lower temperature. These differences would make the spectra steeper, but their effect is canceled by the edges of the system freezing out at a higher temperature.

Next in Fig. 4 we plot the p_T -differential elliptic flow $v_2(p_T)$ of pions and protons at $\sqrt{s_{NN}} = 200$ GeV 20-30% central Au+Au collisions using both EoSs and freeze-out criteria. Since we use an averaged initial state, we have evaluated the elliptic flow with respect to the reaction

³ Later freeze-out, *i.e.* lower freeze-out temperature or larger freeze-out Knudsen number, would make the pion spectrum too soft, see discussions in Refs. [40, 41].

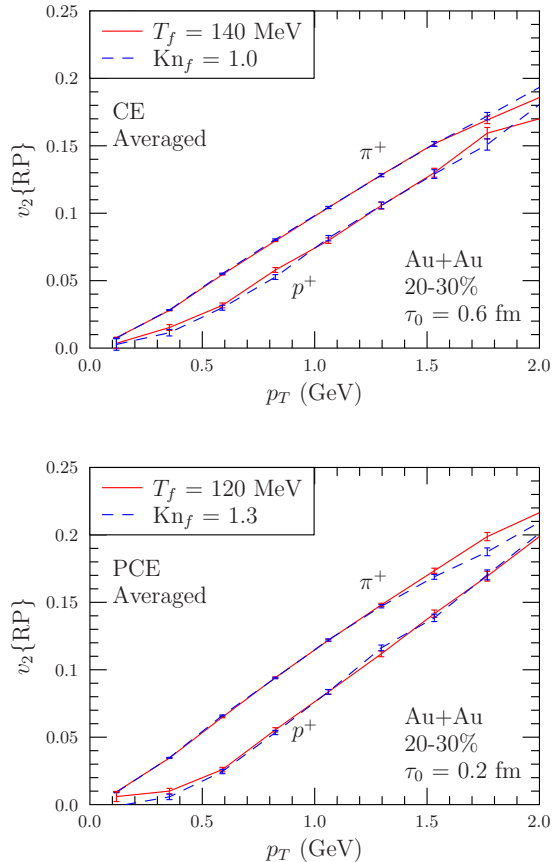


FIG. 4: Elliptic flow of positively charged pions and protons in $\sqrt{s_{NN}} = 200$ GeV 20-30% central Au+Au collisions assuming chemical (top) or partial chemical (bottom) equilibrium in the EoS. The solid red line corresponds to the results obtained using freeze-out at constant temperature and the dashed blue line using freeze-out at constant Knudsen number. Error bars depict estimated statistical errors.

plane, $v_2\{\text{RP}\}$.

In our earlier proceedings contribution [42], we saw that elliptic flow was sensitive to the freeze-out criterion when *s95p*-PCE-v1 EoS was used. However, in that calculation we had fixed $\text{Kn}_f = 1.0$, and the p_T distributions were different as well. Now, after choosing the freeze-out Knudsen number to reproduce the data and the spectra calculated using the constant temperature freeze-out criterion, both freeze-out criteria lead to similar elliptic flow. The same happens also when we keep $\text{Kn}_f = 1.0$ fixed, and adjust the freeze-out temperature instead to $T_f = 140$ MeV to achieve similar spectra.

To study whether the sensitivity to the freeze-out criterion might depend on the initial state, we performed the calculations using pure binary-collision profile as well. We used initial time $\tau_0 = 0.6$ fm, freeze-out temperature $T_f = 120$ MeV, and Knudsen number $\text{Kn}_f = 1.3$ with *s95p*-PCE-v1, and found out that the spectra and elliptic flow were again independent of the freeze-out crite-

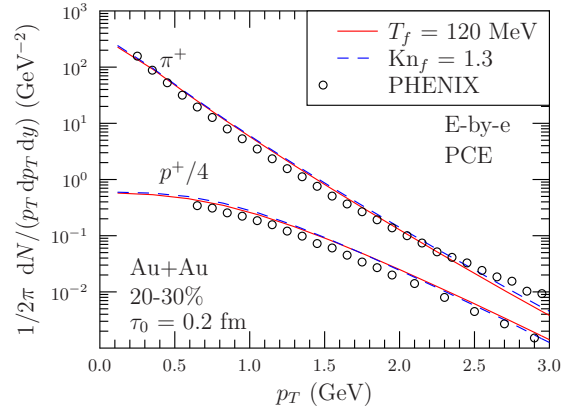


FIG. 5: Transverse momentum spectra of positively charged pions and protons in $\sqrt{s_{NN}} = 200$ GeV 20-30% central Au+Au collisions from event-by-event hydrodynamical simulations. The solid red line corresponds to the results obtained using freeze-out at constant temperature and the dashed blue line using freeze-out at constant Knudsen number. The data are from the PHENIX Collaboration [39].

ron. Thus we suspect that this similarity with both criteria is not due to some property of the initial state but could be a more general phenomenon. Also note that the same pair of constant temperature and Knudsen number worked with both initial states.

B. Event-by-event fluctuating initial states in $\sqrt{s_{NN}} = 200$ GeV Au+Au collisions at RHIC

As argued in the introduction, in event-by-event calculations the two freeze-out criteria might lead to different results, even if the results were similar when averaged initial state was used. To study this assumption, we modeled the collisions at RHIC event-by-event using the chemically frozen *s95p*-PCE-v1 EoS. We followed the same procedure than in our calculations using an averaged initial state, and treated both the freeze-out temperature and Knudsen number as free parameters to be adjusted to reproduce the observed p_T spectra. It turned out that the same combination of parameters, $T_f = 140$ MeV and $\text{Kn}_f = 1.3$, lead to a reasonable reproduction of the data in both event-by-event and averaged initial state calculations, see Figs. 5 and 3, respectively. However, as observed before, e.g. in Ref. [15], the spectra are a little bit flatter in the event-by-event case.

The p_T -differential elliptic and triangular flows are shown in Fig. 6. In event-by-event calculations it makes more sense to calculate the flow coefficients with respect to their event planes, and therefore $v_n\{EP\}$ values are shown in the figures. Consequently comparison to the averaged initial state case cannot be made, because the definitions of flow are different.

Unlike what we expected, there is no significant dif-

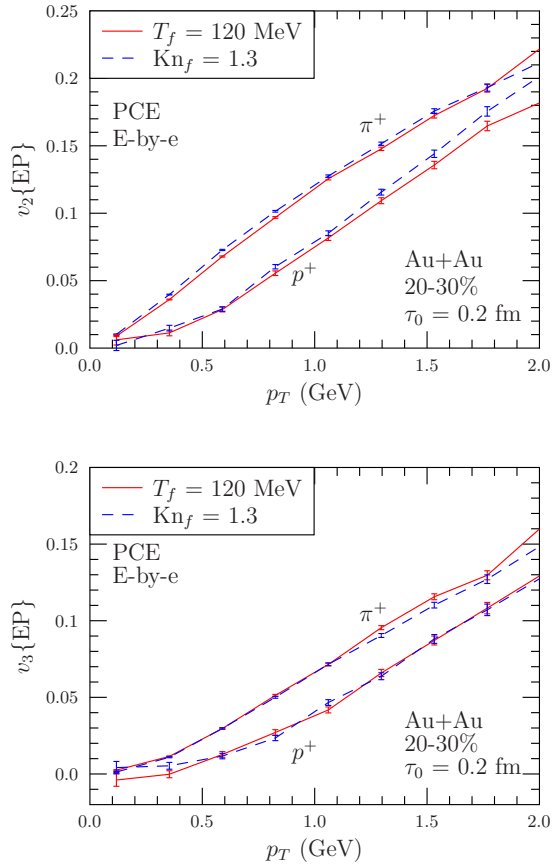


FIG. 6: Elliptic (top) and triangular (bottom) flow of positive pions and protons in $\sqrt{s_{NN}} = 200$ GeV 20-30% central Au+Au collisions from event-by-event hydrodynamical simulations. The solid red line corresponds to the results obtained using freeze-out at constant temperature and the dashed blue line using freeze-out at constant Knudsen number. Error bars depict estimated statistical errors.

ference between the freeze-out criteria. We also checked with smaller number of events that in the most central collisions, where both v_2 and v_3 are generated mostly by fluctuations, the situation is the same. Thus both anisotropies seem to be insensitive to the freeze-out criterion in event-by-event calculation too.

We have also checked that in individual events, the spectra, elliptic flow, and triangular flow are not necessarily the same with the parameters used, but the difference can be of the order of 10% in each studied variable. This opens up the question whether the event-by-event distribution of anisotropies [43] might be sensitive to the freeze-out criterion, and how the freeze-out criterion would affect the correlation between the initial state anisotropy and final momentum anisotropy [43, 44]. We have not checked either what would happen if we adjusted the freeze-out criteria event-by-event so that the p_T distributions were similar in each single event.

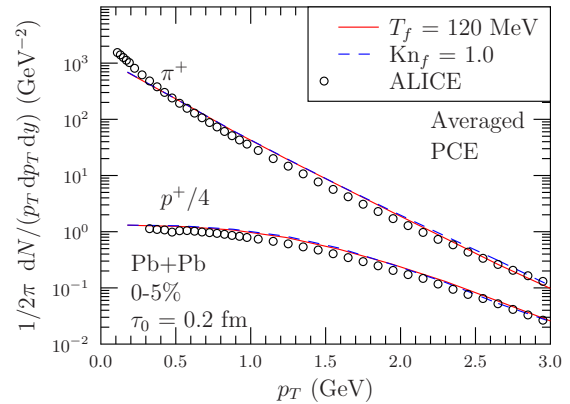


FIG. 7: Transverse momentum spectra of positive pions and protons in $\sqrt{s_{NN}} = 2760$ GeV 0-5% central Pb+Pb collisions. The solid red line corresponds to the results obtained using freeze-out at constant temperature and the dashed blue line using freeze-out at constant Knudsen number. The data are from the ALICE Collaboration [45].

C. Averaged initial state in $\sqrt{s_{NN}} = 2760$ GeV Pb+Pb collisions at the LHC

At a single collision energy one can always fix the freeze-out temperature to reproduce the p_T spectra, but there is no physical reason why the same freeze-out temperature should work at another collision energy. On the other hand, the dynamical criterion with freeze-out at constant Knudsen number is based on local expansion dynamics and general considerations about the validity of hydrodynamics, and therefore we can expect the freeze-out to take place at the same value of Knudsen number independent of the collision energy. Thus it is worthwhile to check what happens in collisions at the LHC energy.

In Fig. 7 we show the transverse momentum spectra of pions and protons in $\sqrt{s_{NN}} = 2760$ GeV 0-5% central Pb+Pb collisions using averaged initial state and $s95p$ -PCE-v1 EoS. Contrary to our expectations, the favored freeze-out temperature was the same $T_f = 120$ MeV both at RHIC and at the LHC, but the data favored lower freeze-out Knudsen number $Kn_f = 1.0$ at the LHC. This may be an effect of neglecting dissipation: When the dynamical criterion of freeze-out at constant Knudsen number was used in the context of dissipative hydro [12], the same freeze-out Knudsen number worked both at RHIC and the LHC. On the other hand, since the slopes of the final p_T distributions depend on the initial pressure gradients, the collision energy dependence of the freeze-out Knudsen number may also indicate that our Glauber based initial state model does not reproduce the initial gradients properly. Thus it would be interesting to apply the dynamical freeze-out criterion to more sophisticated EKRT [44, 46, 47] and IP-Glasma [48, 49] initial states.

The p_T -differential elliptic flow of pions and protons shown in Fig. 8 depicts the same pattern at the LHC

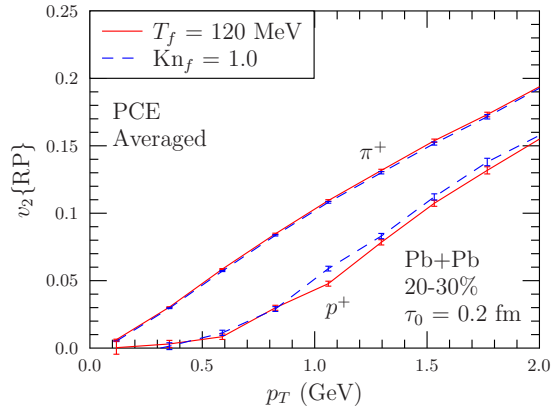


FIG. 8: Elliptic flow of positive pions and protons in $\sqrt{s_{NN}} = 2760$ GeV 20-30% central Pb+Pb collisions. The solid red line corresponds to the results obtained using freeze-out at constant temperature and the dashed blue line using freeze-out at constant Knudsen number. Error bars depict estimated statistical errors.

as at RHIC: Once the p_T spectra are reproduced, both freeze-out criteria lead to similar elliptic flow.

To be sure, we carried out the event-by-event calculations at the LHC energy too, but saw the very same behavior as at RHIC and when using the averaged initial state: Once the freeze-out parameters were chosen to reproduce the observed spectra ($T_f = 120$ MeV and $Kn_f = 1.0$), the elliptic and triangular flows were similar too.

V. CONCLUSIONS

As argued in the introduction, freeze-out criterion based on freeze-out at a constant temperature is an oversimplification, and a dynamical criterion where freeze-out takes place at constant Knudsen number would be more physical. However, we saw that in semi-central and central collisions, identified particle spectra and elliptic and triangular flows are not sensitive to the freeze-out criterion.

We evaluated the Knudsen number as the ratio of the expansion rate of the system, and the scattering rate of pions. We applied the freeze-outs at constant temperature and constant Knudsen number to ideal fluid calculations of Au+Au collisions at RHIC and Pb+Pb collisions at the LHC at 20-30% centrality, and fixed the values of freeze-out parameters by fitting the observed pion and proton p_T distributions. The two criteria lead to different freeze-out surfaces: with dynamical freeze-out the edges decouple earlier (i.e. at higher temperature) and the center of the system lives longer letting the matter cool more compared to the constant temperature case. However, after the p_T spectra were constrained to be similar, no sign of the different temperatures and flow

velocities on the freeze-out surface could be seen in the anisotropies.

We did check that the same insensitivity persists in most central collisions, but we did not check what might happen when the collision system is much smaller like in peripheral A+A or in p+A collisions. The earlier results of Ref. [12] indicate that the sensitivity to the freeze-out criterion increases when the system size or collision energy decreases, and thus the p+A collision system could be very sensitive to the freeze-out criterion. Maybe even to such an extent that the Knudsen number at the very beginning of the evolution is larger than one [6].

Our event-by-event calculations revealed that even if the spectra and anisotropies after averaging over many events were not sensitive to the freeze-out criterion, spectra and anisotropies in individual events were. This leaves open the question whether event-by-event distributions of average p_T or anisotropy coefficients v_n might be sensitive to the freeze-out criterion. One could also expect that HBT radii would be an observable which is more sensitive than the anisotropies to the exact properties of the freeze-out surface.

Unfortunately we were unable to study how the value of the smearing parameter σ of the Monte Carlo Glauber model affects the sensitivity to freeze-out, and thus whether small scale density fluctuations in the initial state might affect the freeze-out. This remains to be explored in a further study, although one may expect that dissipation has largely smeared away small scale structures by the time of freeze-out.

Acknowledgments

Fruitful discussions with S. Bass, M. Bleicher, H. van Hees, H. Honkanen, J. I. Kapusta, A. Kurkela, D. Molnar, B. Tomasik, and R. Venugopalan are gratefully acknowledged. We thank M. A. R. Kaltenborn, M. Marzenko, and H. Niemi for careful reading of the manuscript and constructive comments. PH. thanks for hospitality the Iowa State University and Goethe University where part of this work was done. During the long gestation of this project, the work of PH. has been supported by the Polish Science Foundation (NCN) under Maestro grant DEC-2013/10/A/ST2/00106, BMBF under contract no. 06FY9092, the ExtreMe Matter Institute (EMMI), DOE grant DE-AC02-98CH10886, and Johannes Rättendahl foundation. The works of SA. and HH. have been supported by DOE grant DE-FG02-01ER4120 and the ExtreMe Matter Institute (EMMI), respectively.

Appendix A: Integrals in the calculation of the scattering rate

The reduction of the number of integrals over momentum in the scattering rate calculations has been shown

in Ref. [24] for equal mass particles obeying Boltzmann statistics, and generalized for nonidentical particles when the scattering partner has a fixed momentum in Ref. [21]. For the sake of completeness, we repeat the process here, and generalize it for quantum statistics.

The total number of times pions scatter with particles i per unit volume per unit time is given by:

$$\begin{aligned} \mathcal{R}_i &= 2 \int_{s_a}^{\infty} ds \sqrt{(s-s_a)(s-s_b)} \sigma_{\pi i}(s) \\ &\quad \times \int \frac{d^3 p_\pi}{2E_\pi} \frac{d^3 p_i}{2E_i} f_\pi(T, \mu_\pi) f_i(T, \mu_i) \delta(s - (p_i + p_\pi)^2), \end{aligned} \quad (\text{A1})$$

where, compared to Eq. (2), we have added the integration over center-of-mass energy s and the corresponding δ -function. To proceed we express the distribution functions f_π and f_i as series:

$$\begin{aligned} f_i(T, \mu_i) &= \frac{g_i}{(2\pi)^3} \frac{1}{e^{\frac{E-\mu_i}{T}} \pm 1} \\ &= \frac{g_i}{(2\pi)^3} \sum_{n=1}^{\infty} (\mp 1)^{n+1} e^{n\mu_i/T} e^{-nE/T}, \end{aligned} \quad (\text{A2})$$

where -1 in the series is for fermions and $+1$ for bosons, change the momentum coordinates to spherical coordinates, change the integral over the magnitude of momentum to integral over energy, and rewrite the δ -function as

$$\begin{aligned} &\delta(s - (p_i + p_\pi)^2) \\ &= \frac{1}{2|\mathbf{p}_\pi||\mathbf{p}_i|} \delta\left(\cos\theta_i + \frac{s - (m_\pi^2 + m_i^2) - 2E_\pi E_i}{2|\mathbf{p}_\pi||\mathbf{p}_i|}\right). \end{aligned} \quad (\text{A3})$$

The angular integrals can now be carried out, and we get

$$\begin{aligned} \mathcal{R}_i &= \frac{g_i}{2^5 \pi^4} \sum_{k=1}^{\infty} e^{k\mu_\pi/T} \sum_{n=1}^{\infty} (\mp 1)^{n+1} e^{n\mu_i/T} \\ &\quad \times \int_{s_a}^{\infty} ds \sqrt{(s-s_a)(s-s_b)} \sigma_{\pi i}(s) \\ &\quad \times \int_{m_\pi}^{\infty} dE_\pi \int_{m_i}^{\infty} dE_i e^{-\frac{k}{T}(E_\pi + \frac{n}{k}E_i)} \\ &\quad \times \Theta\left(1 - \left| \frac{s - (m_\pi^2 + m_i^2) - 2E_\pi E_i}{2|\mathbf{p}_\pi||\mathbf{p}_i|} \right| \right). \end{aligned} \quad (\text{A4})$$

We change the integration variables from E_π and E_i to $y = E_\pi + \frac{1}{r}E_i$ and $x = E_\pi - \frac{1}{r}E_i$, where $r = k/n$. The Θ function constraint can now be written as $b < x < c$,

where

$$\begin{aligned} b &= \frac{(r^2 m_\pi^2 - m_i^2)y - d}{rs - (r-1)(m_i^2 - rm_\pi^2)} \\ c &= \frac{(r^2 m_\pi^2 - m_i^2)y + d}{rs - (r-1)(m_i^2 - rm_\pi^2)} \\ d &= \sqrt{r^2 y^2 - (rs - (r-1)(m_i^2 - rm_\pi^2))} \\ &\quad \times \sqrt{(s-s_a)(s-s_b)}. \end{aligned} \quad (\text{A5})$$

It turns out that the integration over x is constrained more by the Θ function than by the integration limits, and we get

$$\begin{aligned} \mathcal{R}_i &= \frac{g_i}{2^6 \pi^4} \sum_{k=1}^{\infty} e^{k\mu_\pi/T} \sum_{n=1}^{\infty} (\mp 1)^{n+1} e^{n\mu_i/T} \\ &\quad \times r \int_{s_a}^{\infty} ds \sqrt{(s-s_a)(s-s_b)} \sigma_{\pi i}(s) \\ &\quad \times \int_{\alpha}^{\infty} dy e^{-\frac{ky}{T}} (c-b), \end{aligned} \quad (\text{A6})$$

where

$$\alpha = \sqrt{\frac{s}{r} - \frac{r-1}{r^2} (m_i^2 - rm_\pi^2)}. \quad (\text{A7})$$

The y integral can now be reordered and carried out to be

$$\int_{\alpha}^{\infty} dy e^{-k\frac{y}{T}} \sqrt{y^2 - \alpha^2} = \frac{T\alpha}{k} K_1\left(\frac{k\alpha}{T}\right), \quad (\text{A8})$$

where K_1 is the modified Bessel function. Inserting this into Eq. (A6) and keeping the y independent terms omitted from Eq. (A8), we finally get

$$\begin{aligned} \mathcal{R}_i &= \frac{g_i T}{2^5 \pi^4} \sum_{k=1}^{\infty} e^{k\mu_\pi/T} \sum_{n=1}^{\infty} \frac{(\mp 1)^{n+1}}{n} e^{n\mu_i/T} \\ &\quad \times \int_{s_a}^{\infty} ds \frac{(s-s_a)(s-s_b) \sigma_{\pi i}(s)}{\sqrt{rs - (r-1)(m_i^2 - rm_\pi^2)}} \\ &\quad \times K_1\left(\frac{n}{T} \sqrt{rs - (r-1)(m_i^2 - rm_\pi^2)}\right). \end{aligned} \quad (\text{A9})$$

After summing over all particles i , and dividing by pion density, we get Eq. (3).

Appendix B: Center of mass momentum in particle-resonance scattering

If one of the scattering partners is a resonance, the conventional expression for the center-of-mass momentum of the scattering,

$$\begin{aligned} p_{\text{cms}} &(\sqrt{s}, m_1, m_2) \\ &= \frac{\sqrt{(s - (m_1 + m_2)^2)(s - (m_1 - m_2)^2)}}{2\sqrt{s}}, \end{aligned} \quad (\text{B1})$$

must be amended to take into account the finite width of the resonance. To do this, we again mostly follow the UrQMD description [26], and include an integral over the mass distribution of the resonance:

$$p_{\text{cms}}(\sqrt{s}) = \int_0^{\sqrt{s}-m_\pi} dm p_{\text{CMS}}(\sqrt{s}, m_\pi, m) \times \frac{1}{2\pi} \frac{\Gamma_R}{(m_R - m)^2 + \Gamma_R^2/4}, \quad (\text{B2})$$

where we assume the mass distribution to be the Breit-Wigner distribution with mass-independent width Γ_R , and m_R is the pole mass of the resonance.

Note that, in the integrals of Appendix A, and in the evaluation of the EoS, the resonances have been assumed to have zero width, and their pole masses have been used as their masses.

Appendix C: Full decay width

The evaluation of the full decay width $\Gamma_{\text{tot}}(M)$ in Eq. (4) requires knowledge of partial decay widths of three- and four-body decay channels as well. Unfortunately Eq. (5) cannot be easily generalized to many-body

decays. To treat all decay channels in a similar fashion, we combine the particles in three- and four-body decays into a particle and a particle pair, or two particle pairs, respectively, use the invariant mass(es) of particle pair(s) to evaluate the center-of-mass momentum (Eq. (B1)), and use the available phase space to give the mass distribution of the invariant mass of the pair(s). In particular, for three-body decays we obtain:

$$p_{\text{cms}}(M) = \frac{8M}{N} \int_{m_1+m_2}^{M-m_3} dm_{\text{pair}} [p_{\text{cms}}(M, m_{\text{pair}}, m_3)]^2 \times p_{\text{cms}}(m_{\text{pair}}, m_1, m_2), \quad (\text{C1})$$

where the normalization factor N is given by

$$N = 8M \int_{m_1+m_2}^{M-m_3} dm_{\text{pair}} p_{\text{cms}}(M, m_{\text{pair}}, m_3) \times p_{\text{cms}}(m_{\text{pair}}, m_1, m_2). \quad (\text{C2})$$

If any of the daughter particles in a multi-particle decay is a resonance, we use its pole mass only and neglect its width.

-
- [1] U. W. Heinz and R. Snellings, *Annu. Rev. Nucl. Part. Sci.* **63**, 123 (2013) [arXiv:1301.2826 [nucl-th]].
- [2] C. Gale, S. Jeon and B. Schenke, *Int. J. Mod. Phys. A* **28**, 1340011 (2013) [arXiv:1301.5893 [nucl-th]].
- [3] H. Niemi, *Nucl. Phys. A* **931**, 227 (2014).
- [4] P. F. Kolb and U. W. Heinz, in *Quark-Gluon Plasma 3*, edited by R. C. Hwa and X.-N. Wang (World Scientific, Singapore, 2004), p. 634 [nucl-th/0305084].
- [5] U. W. Heinz, K. S. Lee and E. Schnedermann, in *Quark-Gluon Plasma*, edited by R. C. Hwa (World Scientific, Singapore, 1990), p. 471.
- [6] H. Niemi and G. S. Denicol, arXiv:1404.7327 [nucl-th].
- [7] J. P. Bondorf, S. I. A. Garpman and J. Zimanyi, *Nucl. Phys. A* **296**, 320 (1978).
- [8] I. N. Mishustin and L. M. Satarov, *Sov. J. Nucl. Phys.* **37**, 532 (1983) [*Yad. Fiz.* **37**, 894 (1983)].
- [9] C. M. Hung and E. V. Shuryak, *Phys. Rev. C* **57**, 1891 (1998) [hep-ph/9709264].
- [10] U. Heinz and G. Kestin, *PoS CPOD* **2006**, 038 (2006) [nucl-th/0612105].
- [11] K. J. Eskola, H. Niemi and P. V. Ruuskanen, *Phys. Rev. C* **77**, 044907 (2008) [arXiv:0710.4476 [hep-ph]].
- [12] E. Molnar, H. Holopainen, P. Huovinen and H. Niemi, *Phys. Rev. C* **90**, 044904 (2014) [arXiv:1407.8152 [nucl-th]].
- [13] D. H. Rischke, *Lect. Notes Phys.* **516**, 21 (1999) [nucl-th/9809044].
- [14] E. Schnedermann and U. W. Heinz, *Phys. Rev. C* **50**, 1675 (1994) [nucl-th/9402018].
- [15] H. Holopainen, H. Niemi, and K. Eskola, *Phys. Rev. C* **83**, 034901 (2011) [arXiv:1007.0368 [hep-ph]].
- [16] D. Oliinychenko, P. Huovinen and H. Petersen, *Phys. Rev. C* **91**, 024906 (2015) [arXiv:1411.3912 [nucl-th]].
- [17] D. Oliinychenko, P. Huovinen and H. Petersen, *J. Phys. Conf. Ser.* **599**, no. 1, 012017 (2015) [arXiv:1412.2020 [nucl-th]].
- [18] T. Hirano, P. Huovinen, K. Murase and Y. Nara, *Prog. Part. Nucl. Phys.* **70**, 108 (2013) [arXiv:1204.5814 [nucl-th]].
- [19] H. Petersen, *J. Phys. G* **41**, no. 12, 124005 (2014) [arXiv:1404.1763 [nucl-th]].
- [20] P. Huovinen and H. Petersen, *Eur. Phys. J. A* **48**, 171 (2012) [arXiv:1206.3371 [nucl-th]].
- [21] B. Tomasik and U. A. Wiedemann, *Phys. Rev. C* **68**, 034905 (2003) [nucl-th/0207074].
- [22] J. Ftacnik, P. Lichard, N. Pisutova and J. Pisut, *Z. Phys. C* **42**, 139 (1989).
- [23] M. Prakash, M. Prakash, R. Venugopalan and G. Welke, *Phys. Rept.* **227**, 321 (1993).
- [24] B. Zhang, M. Gyulassy and Y. Pang, *Phys. Rev. C* **58**, 1175 (1998) [nucl-th/9801037].
- [25] P. Huovinen and P. Petreczky, *Nucl. Phys. A* **837**, 26 (2010) [arXiv:0912.2541 [hep-ph]].
- [26] S. A. Bass *et al.*, *Prog. Part. Nucl. Phys.* **41**, 255 (1998) [nucl-th/9803035].
- [27] M. Bleicher *et al.*, *J. Phys. G* **25**, 1859 (1999) [hep-ph/9909407].
- [28] S. Eidelman *et al.* [Particle Data Group], *Phys. Lett. B* **592**, 1 (2004).
- [29] R. G. Daghigh and J. I. Kapusta, *Phys. Rev. D* **65**, 064028 (2002) [gr-qc/0109090].
- [30] J. P. Boris and D. L. Book, *J. Comput. Phys.* **11**, 38 (1973).
- [31] C. R. DeVore, *J. Comput. Phys.* **92**, 142 (1991).

- [32] S. T. Zalesak, *J. Comput. Phys.* **31**, 248 (1979).
- [33] A. Dumitru, *Phys. Lett. B* **463**, 138 (1999) [hep-ph/9905217].
- [34] M. Alvioli, H. Holopainen, K. J. Eskola and M. Strikman, *Phys. Rev. C* **85**, 034902 (2012) [arXiv:1112.5306 [hep-ph]].
- [35] G. S. Denicol, C. Gale, S. Jeon, J.-F. Paquet and B. Schenke, arXiv:1406.7792 [nucl-th].
- [36] B. I. Abelev *et al.* [STAR Collaboration], *Phys. Rev. C* **79**, 034909 (2009) [arXiv:0808.2041 [nucl-ex]].
- [37] K. Aamodt *et al.* [ALICE Collaboration], *Phys. Rev. Lett.* **106**, 032301 (2011) [arXiv:1012.1657 [nucl-ex]].
- [38] H. Holopainen and P. Huovinen, *J. Phys. Conf. Ser.* **389**, 012018 (2012) [arXiv:1207.7331 [hep-ph]].
- [39] S. S. Adler *et al.* (PHENIX Collaboration), *Phys. Rev. C* **69**, 034909 (2004) [nucl-ex/0307022].
- [40] T. Hirano and M. Gyulassy, *Nucl. Phys. A* **769**, 71 (2006) [nucl-th/0506049].
- [41] P. Huovinen, *Eur. Phys. J. A* **37**, 121 (2008) [arXiv:0710.4379 [nucl-th]].
- [42] H. Holopainen and P. Huovinen, *J. Phys. Conf. Ser.* **509**, 012114 (2014) [arXiv:1310.0347 [nucl-th]].
- [43] H. Niemi, G. S. Denicol, H. Holopainen and P. Huovinen, *Phys. Rev. C* **87**, 054901 (2013) [arXiv:1212.1008 [nucl-th]].
- [44] H. Niemi, K. J. Eskola and R. Paatelainen, *Phys. Rev. C* **93**, 024907 (2016) [arXiv:1505.02677 [hep-ph]].
- [45] B. Abelev *et al.* (ALICE Collaboration), *Phys. Rev. Lett.* **109**, 252301 (2012) [arXiv:1208.1974 [hep-ex]].
- [46] K. J. Eskola, K. Kajantie, P. V. Ruuskanen and K. Tuominen, *Nucl. Phys. B* **570**, 379 (2000) [hep-ph/9909456].
- [47] R. Paatelainen, K. J. Eskola, H. Holopainen and K. Tuominen, *Phys. Rev. C* **87**, 044904 (2013) [arXiv:1211.0461 [hep-ph]].
- [48] B. Schenke, P. Tribedy and R. Venugopalan, *Phys. Rev. Lett.* **108**, 252301 (2012) [arXiv:1202.6646 [nucl-th]].
- [49] B. Schenke, P. Tribedy and R. Venugopalan, *Phys. Rev. C* **86**, 034908 (2012) [arXiv:1206.6805 [hep-ph]].